Fermionic warm dark matter produces galaxy cores in the observed scales because of quantum mechanics

C. Destri[a], H. J. de Vega[b,c,1], N. G. Sanchez[c]

[a]*Dipartimento di Fisica G. Occhialini, Università Milano-Bicocca and INFN, sezione di Milano-Bicocca, Piazza della Scienza 3, 20126 Milano, Italia.*
[b]*LPTHE, Université Pierre et Marie Curie (Paris VI), Laboratoire Associé au CNRS UMR 7589, Tour 13-14, 4ème. et 5ème. étage, Boîte 126, 4, Place Jussieu, 75252 Paris, Cedex 05, France*
[c]*Observatoire de Paris, LERMA, Laboratoire Associé au CNRS UMR 8112, 61, Avenue de l'Observatoire, 75014 Paris, France*

Abstract

We derive the main physical galaxy properties: mass, halo radius, phase space density and velocity dispersion from a semiclassical gravitational approach in which fermionic WDM is treated quantum mechanically. They turn out to be fully compatible with observations. The Pauli Principle implies for the fermionic DM phase-space density $Q(\vec{r}) = \rho(\vec{r})/\sigma^3(\vec{r})$ the quantum bound $Q(\vec{r}) \leq K\ m^4/\hbar^3$, where m is the DM particle mass, $\sigma(\vec{r})$ is the DM velocity dispersion and K is a pure number of order one which we estimate. Cusped profiles from N-body galaxy simulations produce a divergent $Q(r)$ at $r = 0$ violating this quantum bound. The combination of this quantum bound with the behaviour of $Q(r)$ from simulations, the virial theorem and galaxy observational data on Q implies lower bounds on the halo radius and a minimal distance r_{min} from the centre at which classical galaxy dynamics for DM fermions breaks down. For WDM, r_{min} turns to be in the parsec scale. For cold dark matter (CDM), r_{min} is between dozens of kilometers and a few meters, astronomically compatible with zero. For hot dark matter (HDM), r_{min} is from the kpc to the Mpc. In summary, this quantum bound rules out the presence of galaxy cusps for fermionic WDM, in agreement with astronomical observations, which show that the DM halos are cored. We show that compact dwarf galaxies are natural quantum macroscopic objects supported against gravity by the fermionic WDM quantum pressure (quantum degenerate fermions) with a minimal galaxy mass and minimal velocity dispersion. Quantum mechanical calculations which fulfil the Pauli principle become necessary to compute galaxy structures at kpc scales and below. Classical N-body simulations are not valid at scales below r_{min}. We apply the Thomas-Fermi semiclassical approach to fermionic WDM galaxies, we resolve it numerically and find the physical galaxy magnitudes: mass, halo radius, phase-space density, velocity dispersion, fully consistent with observations especially for compact dwarf galaxies. Namely, fermionic WDM treated quantum mechanically, as it must be, reproduces the observed galaxy DM cores and their sizes. The lightest known dwarf galaxy (Willman I) implies a lower bound for the WDM particle mass $m > 0.96$ keV. These results and the observed galaxies with halo radius ≥ 30 pc and halo mass $\geq 4 \times 10^5\ M_\odot$ provide further indication that the WDM particle mass m is approximately in the range 1-2 keV.

Keywords: cosmology: dark matter, galaxies: halos, galaxies: kinematics and dynamics

1. Introduction and summary of results

Dark matter (DM) is the main component of galaxies, especially of dwarf galaxies which are almost exclusively formed by DM. It thus appears that studying galaxy properties is an excellent way to disentangle the nature of DM.

Cold DM (CDM) produces an overabundance of substructures below the $\sim$ 50 kpc till very small scales $\sim$ 0.005 pc which constitutes, as is well known, one of the most serious drawbacks for CDM. On the contrary, warm DM (WDM), that is, DM particles with mass in the keV scale, produces DM structures in the observed range of scales $\gtrsim$ 50 kpc. In WDM structure formation, substructures below the free-streaming scale $\sim$ 50 kpc are not formed contrary to the case of CDM. This conclusion for WDM based on the linear theory is confirmed by N-body simulations [12, 23, 56, 58, 47, 36, 72]. For scales larger than 50 kpc, WDM yields the same results than CDM and agrees with all the observations.

Astronomical observations show that the DM galaxy density profiles are **cored** till scales below the kpc [71, 61, 50, 15, 24, 65]. On the other hand, N-body CDM simulations exhibit cusped density profiles with a typical $1/r$ behaviour near the galaxy center $r = 0$. WDM simulations exhibit cusps or small cores smaller than the observed cores [2, 13, 63, 64].

Numerical calculations on the spherically symmetric Vlasov–Poisson equation based on the Larson moment expansion [34, 33], as well as on the exact dynamics of the associated N-body system, have confirmed these findings [17].

For fermionic DM the Pauli principle states that the phase-space distribution function for spin-$\frac{1}{2}$ particles $f(\vec{r}, \vec{p})$ must be smaller than two

$$f(\vec{r}, \vec{p}) \leq 2 \, . \tag{1}$$

Since the matter density $\rho(\vec{r})$ is obtained from the phase-space distribution through

$$\rho(\vec{r}) = m \int d^3p \, \frac{f(\vec{r}, \vec{p})}{(2\,\pi\,\hbar)^3} \quad , \quad m = \text{DM particle mass} \, , \tag{2}$$

this implies a bound on the phase-space density $Q(\vec{r}) \equiv \rho(\vec{r})/\sigma^3(\vec{r})$ where $\sigma(\vec{r})$ is the DM velocity dispersion, which takes the form (see sec. 2)

$$\frac{\hbar^3}{m^4} \, Q(\vec{r}) \leq K \, . \tag{3}$$

Here K is a pure number of order one that we estimate in appendix Appendix A and display in Table 1. In the classical physics limit $\hbar \to 0$, the right hand side goes to infinity and the bound on $Q(\vec{r})$ disappears.

The quantum bound eq.(1) in the cosmological context has been previously considered in refs. [59, 25, 26] to derive lower bounds on neutral lepton masses. In the present paper, we use this bound in a new way incorporating the behaviour of the phase-space density $Q(r)$ [1, 27, 37, 62, 45] and observational data to derive lower bounds on the halo radius. These bounds

[1]Corresponding author. H. J. de Vega, devega@lpthe.jussieu.fr, Tel. 33-1-4427-7394, Fax 33-1-4427-7393

are of semiclassical gravitational nature and motivate us to use the Thomas-Fermi approach for galaxies, namely, treating gravitation classically and fermionic WDM quantum mechanically.

We combine the quantum bound eq.(3) with the results from classical N-body simulations which indicate a simple power law behaviour for $Q(r)$ [1, 27, 37, 62, 45]

$$Q(r) = Q_h \left(\frac{r}{r_h}\right)^{-\beta} \tag{4}$$

where $\beta \simeq 1.9 - 2$, r_h is the halo radius and Q_h stands for the mean phase space density in the halo. Classical WDM N-body simulations yield results similar to the behaviour eq.(4) even for $r \lesssim r_h$, when properly using the velocity dispersion of the keV-scale WDM particles [38, 51].

Classically, $Q(r)$ grows unbounded for $r \to 0$ violating the quantum bound eq.(3). Therefore, for small enough scales classical physics in galaxies **breaks down**. In other words, classical N-body simulations and hydrodynamical simulations are not applicable near the galaxy centers.

We show that the classical result eq.(4) only holds for distances far enough from the galaxy center, namely for

$$r \geq r_{min} \equiv \frac{\hbar^{\frac{3}{2}}}{m^2} \sqrt{\frac{Q_h}{K}}\, r_h \ . \tag{5}$$

For a DM particle mass in the keV scale and the observed values of r_h and Q_h, it turns out that r_{min} can be between 0.1 and 1 pc.

Eq.(5) provides the **minimal** distance from the center where quantum mechanical effects are **essential** and rules out the presence of galaxy cusps for fermionic WDM. Moreover, quantum mechanical effects extend well beyond $r = r_{min}$ because smoothing up the classical cusp which sucks matter towards the origin has an effect on the whole galaxy halo.

Taking into account the quantum nature of fermionic DM introduces a physical length scale of quantum origin. As a consequence, density profiles become regular (cored) at the origin. For bosonic DM, the bound eq.(13) does not apply and the formation of cusps is allowed. However, the observed galaxy density profiles are cored [71, 61, 50, 15, 24, 65].

The quantum bound eq.(13) applies for any kind of fermionic dark matter with the value of r_{min} determined by the DM particle mass. For CDM where 1 GeV $< m <$ 100 GeV, r_{min} is between dozens of kilometers and a few meters, astronomically compatible with zero. Therefore, classical approaches as N-body simulations and the classical Boltzmann-Vlasov equation fully apply for CDM and unavoidably produce cusps.

HDM where 1 eV $< m <$ 10 eV, suppresses all structures scales below the Mpc scale due to its long free-streaming length and has been ruled out years ago. Anyway, we find that classical aproaches to fermionic HDM as N-body simulations are not valid for scales below an r_{min} which turns to be between the kpc and the Mpc, depending on the galaxy type.

A direct way to see whether a system of particles has a classical or quantum nature is to compare the particle de Broglie wavelength λ_{dB} with the interparticle distance d. We do that in sec. 3.1 and express their ratio as

$$\mathcal{R} \equiv \frac{\lambda_{dB}}{d} = \hbar \left(\frac{Q_h}{m^4}\right)^{\frac{1}{3}} \ .$$

The observed values of Q_h from Table 2 yields

$$2 \times 10^{-3} < \mathcal{R} \left(\frac{m}{\text{keV}}\right)^{\frac{4}{3}} < 1.4 \, . \tag{6}$$

The larger value of $\mathcal{R}$ is for ultracompact dwarfs and the smaller value of $\mathcal{R}$ is for big spirals. The values of $\mathcal{R}$ around unity clearly imply (and solely from observations) that compact dwarf galaxies are natural *macroscopic quantum objects* for WDM.

WDM fermions always provide at least a pressure of quantum nature. When this quantum pressure is balanced with the gravitation pressure, we find values for the total mass $M \sim 10^6 \, M_\odot$, the radius $R \sim 30$ pc and the velocity dispersion $\sigma \sim 2$ km/s consistent with compact dwarf galaxies (see Table 2). These results back the idea that dwarf spheroidal galaxies are supported by the fermionic *WDM quantum pressure*.

We then treat the self-gravitating fermionic DM in the Thomas-Fermi approximation. In this approach, the DM chemical potential $\mu(r) = \mu_0 - m \, \phi(r)$, where μ_0 is a constant and $\phi(r)$ the gravitational potential, obeys the Poisson equation

$$\frac{d^2\mu}{dr^2} + \frac{2}{r} \, \frac{d\mu}{dr} = -\frac{4\,\pi \, G \, m^2}{\pi^2 \, \hbar^3} \int_0^\infty p^2 \, dp \; f\,(e(p) - \mu(r)) \tag{7}$$

where G is Newton's gravitational constant, p is the DM particle momentum, $e(p) = p^2/(2\,m)$ is the DM particle kinetic energy and $f(E)$ is the energy distribution function,

This is a semiclassical gravitational approach to determine selfconsistently the gravitational potential of the fermionic WDM given its distribution function f.

In order to have bounded DM mass densities according to eq.(3) we impose the boundary condition at the origin: $\mu'(0) = 0$.

The distribution function $f(E)$ is determined by the DM evolution since decoupling. Such evolution must take into account the quantum character that emerges when the distribution function approaches the quantum upper bound eq.(3). Such quantum dynamical calculation is beyond the scope of the present paper. We modelize here the distribution function $f(E)$ by the equilibrium Fermi-Dirac distributions and by out of equilibrium distributions for sterile neutrinos (see the appendix Appendix A).

We get a one parameter family of solutions of eqs.(7) parametrized by the value of the chemical potential at the origin $\mu(0)$. We then express the chemical potential at the origin in terms of the phase-space density at the origin $Q(0)$. Large positive values of $\mu(0)$ correspond to the quantum degenerate fermions limit, while large negative values of $\mu(0)$ yield the dilute (classical) limit.

We show that the Thomas-Fermi equation implies the local equation of state

$$P(r) = \frac{1}{3} \, v^2(r) \, \rho(r) \;\; ,$$

and the hydrostatic equilibrium equation

$$\frac{dP}{dr} + \rho(r) \, \frac{d\phi}{dr} = 0 \, .$$

This local equation of state generalizes the local perfect fluid equation for r-dependent velocity $v(r)$.

In the quantum degenerate fermions limit, the halo radius, the velocity dispersion and the galaxy mass take their *minimum* values. These minimum values are similar to the estimates for degenerate fermions given in sec. 3.2.

The masses of compact dwarf spheroidal galaxies dominated by DM must be larger than this minimum mass M_{min}. The lightest known galaxy of this kind is Willman I (see Table 2). Imposing $M_{min} < M_{Willman\ I} = 3.9\ 10^5\ M_\odot$ provides a lower bound for the WDM particle mass:

$$m > 0.96 \text{ keV} . \tag{8}$$

The numerical resolution of eqs.(7) for the whole range of the chemical potential at the origin $\mu(0)$ yields the physical galaxy magnitudes: mass, halo radius, phase-space density and velocity dispersion fully compatible with observations especially for compact dwarf galaxies as can be seen from figs. 1 and 2 and Table 2.

Approaching the classical diluted limit yields larger and larger halo radii, galaxy masses and velocity dispersions. Their maximum values are limited by the initial conditions provided by the primordial power spectrum which determines the sizes and masses of the galaxies formed.

The phase space density decreases from its maximum value for the compact dwarf galaxies corresponding to the degenerate fermions limit till its smallest value for large galaxies (spirals and ellipticals) corresponding to the classical dilute regime.

The theoretical values for r_h, M and $v(0)$ from the Thomas-Fermi approach vary very little with the specific form of the phase-space distribution function $f(E)$ as function of the energy (Fermi-Dirac distribution or out of equilibrium sterile neutrino distribution).

Comparison of the theoretically derived galaxy masses with the galaxy data in fig. 2 indicates a WDM particle mass m approximately in the range 1 - 2 keV. For larger masses, $m \gg 1$ keV an overabundance of small galaxies (small scale structures) without observable counterpart appears.

In summary, the theoretical Thomas-Fermi results are fully consistent with all the observations especially for dwarf compact galaxies as can be seen from figs. 1 and 2. It is highly remarkably that in the context of fermionic WDM the simple static quantum description provided by Thomas-Fermi is able to reproduce such broad variety of galaxies.

These results indicate that fermionic WDM treated quantum mechanically (even approximately) is fully consistent with the observed galaxy properties including the DM core sizes.

Therefore, the effect of including baryons is expected to be a correction to the pure WDM results presented in this paper, consistent with the fact that dark matter is in average six times more abundant than baryons.

In section 2 we describe the quantum bound for the phase-space density of fermionic DM and we derive the relevant galaxy scales where DM classical physics in galaxies breaks down. In section III we show how the quantum fermionic WDM pressure balances the gravitational pressure in galaxies. In section IV the Thomas-Fermi approach for self-gravitating fermionic WDM is presented and applied to galaxies, showing that fermionic WDM treated quantum mechanically is able to reproduce the observed DM properties of galaxies including the DM cores and their sizes. We derive in Appendix A the numerical values of the constant K in the quantum bound for several momentum distributions.

We use units where the speed of light is taken $c = 1$ along this paper.

2. Quantum bounds for fermionic DM in galaxies from the Pauli principle

For fermionic DM the Pauli principle tells us that the number of spin states in a phase-space cell volume $(2\,\pi\,\hbar)^3$ cannot be larger than 2 for spin-$\frac{1}{2}$ particles. Namely, the phase space distribution function $f(\vec{r},\vec{p})$ must satisfy

$$f(\vec{r},\vec{p}) \leq 2\ . \tag{9}$$

The DM number density can be expressed as

$$n(\vec{r}) = \int d^3p\ \frac{f(\vec{r},\vec{p})}{(2\,\pi\,\hbar)^3} = \frac{m^3}{2\,\hbar^3}\ \sigma^3(\vec{r})\ \bar{f}(\vec{r})\ K\ , \tag{10}$$

where $\bar{f}(\vec{r})$ is the maximal $\vec{p}-$average of the phase space distribution over a volume $m^3\ \sigma^3(\vec{r})$, m is the mass of the DM particle, $\sigma(\vec{r})$ is the DM velocity dispersion, $\sigma^2(\vec{r}) \equiv < v^2(\vec{r}) > /3$ and K is a pure number of order one. In appendix Appendix A we evaluate K for distributions of cosmological relevance and display it in Table 1.

We find from eq.(10)

$$\bar{f}(\vec{r}) = \frac{2\ \hbar^3}{K\ m^3}\ \frac{n(\vec{r})}{\sigma^3(\vec{r})} \tag{11}$$

Inserting eq.(11) into eq.(9) which also applies to $\bar{f}(\vec{r})$ yields,

$$\frac{n(\vec{r})}{\sigma^3(\vec{r})} \leq \frac{K\ m^3}{\hbar^3}\ . \tag{12}$$

As a consequence, we find the following bound for the phase-space density:

$$Q(\vec{r}) \equiv \frac{\rho(\vec{r})}{\sigma^3(\vec{r})} \leq K\ \frac{m^4}{\hbar^3}\ . \tag{13}$$

where $\rho(\vec{r}) = m\ n(\vec{r})$ is the matter density. Therefore, the phase space density $Q(\vec{r})$ can **never** take values larger than the right hand side of eq.(13). This is an absolute quantum upper bound which is due to quantum physics, namely the Pauli principle.

In the classical physics limit $\hbar \to 0$ the right hand side of eq.(13) tends to infinity and the bound disappears.

Since the squared velocity dispersion cannot be larger than the speed of light we have a lower bound for the phase-space density

$$Q \geq Q_{min} \equiv 3\ \sqrt{3}\,\rho\ .$$

The upper bound eq.(13) on Q implies, at given density ρ, a lower bound v_{min} on the velocity

$$Q_{max} = 3\ \sqrt{3}\ \frac{\rho}{v_{min}^3} = K\ \frac{m^4}{\hbar^3}\ .$$

and therefore

$$v \geq v_{min} = \hbar\ \sqrt{3}\ \left(\frac{\rho}{K\ m^4}\right)^{\frac{1}{3}} \tag{14}$$

Distribution Function	$\frac{1}{\psi(0)}$	K	$\frac{0.60364}{\sqrt{K}}$
Fermi-Dirac and DW	$3\,\zeta(3) = 3.60617$	1.89858	0.43809
ν-MSM	$0.045\,\pi\,\zeta(5) = 0.14659$	0.077178	2.17285
Maxwell-Boltzmann	$\sqrt{\frac{\pi}{2}} = 1.2533$	0.65985	0.74311

Table 1: The constant K defined by eq.(13) and $0.60364/\sqrt{K}$. We see that the characteristic size is larger for sterile neutrinos decoupling out of equilibrium.

N-body simulations [1, 27, 37, 62, 45] as well as the resolution of Larson's equations [17] point to a cuspy phase-space density behaviour

$$Q(r) = Q_h \left(\frac{r}{r_h}\right)^{-\beta} \tag{15}$$

where $\beta \simeq 1.9 - 2$, r_h is the halo radius and Q_h stands for the mean or characteristic phase space density in the halo. Classical WDM N-body simulations yield results similar to the behaviour eq.(4) even for $r \lesssim r_h$ when properly using the velocity dispersion of the keV-scale WDM particles [38, 51].

We see that this $Q(r)$ derived within classical physics tends to infinity for $r \to 0$ violating the Pauli principle bound eq.(13). Therefore, classical physics in galaxies breaks down near the galaxy center.

Setting $\beta = 2$ for simplicity, we find by combining eqs.(13) and (15)

$$r \geq r_{min} \equiv \frac{\hbar^{\frac{3}{2}}}{m^2}\,\sqrt{\frac{Q_h}{K}}\,r_h\ . \tag{16}$$

That is, $r > r_{min}$ given by eq.(16) sets the domain of validity of classical physics in DM dominated galaxies.

The quantum bound eq.(13) rules out the presence of galaxy cusps for $r \lesssim r_{min}$ and implies the existence of galaxy cores with size larger than r_{min}.

The values of r_h and Q_h vary several orders of magnitude according to the type of the galaxy (see Table 2). Q_h is larger for dwarf spheroids than for spiral galaxies. From Table 2

$$10^{-4} < \frac{\hbar^{\frac{3}{2}}\,\sqrt{Q_h}}{(\mathrm{keV})^2} < 1.3 \tag{17}$$

The larger value corresponds to ultra compact dwarf spheroidals and the smaller one to spiral galaxies. We finally have from eqs. (16) and (17),

$$\frac{10^{-4}}{\sqrt{K}}\left(\frac{\mathrm{keV}}{m}\right)^2 < \frac{r_{min}}{r_h} < \frac{1.3}{\sqrt{K}}\left(\frac{\mathrm{keV}}{m}\right)^2 \ . \tag{18}$$

r_h goes from $\sim$ 10 pc for ultra compact dwarf spheroidals till the 10 kpc range for spiral galaxies.

The right hand larger value in eq.(18) corresponds to the smaller galaxies (ultra compact dwarfs) with r_h in the 10 pc range. The left hand smaller value in eq.(18) corresponds to the larger galaxies (spirals) with r_h in the 10 kpc range. Multiplying both sides of eq.(18) by r_h we obtain for a DM particle mass in the keV scale:

$$0.1 \ \mathrm{pc} \lesssim r_{min} \lesssim 1 \ \mathrm{pc} \ , \tag{19}$$

because r_h is larger for the more dilute galaxies where Q_h is smaller and vice versa.

Notice that eq.(16) provides the **minimal** size of the region where quantum mechanical effects are strong. Quantum mechanical effects will influence a region well beyond the lower bound r_{min}. Namely, removing the classical cusp which sucks matter towards the origin has an effect on the whole galaxy halo.

The quantum bound eq.(9) in the cosmological context has been previously considered in refs. [59, 25, 26] to derive lower bounds on neutral lepton masses. In the present paper, we incorporate to this bound the behaviour of the phase-space density $Q(r)$ [1, 27, 37, 62, 45] to derive lower bounds to the halo radius eq.(16). These bounds are of semiclassical gravitational nature.

Assuming, as usual, that virialization holds within the radius r_h, namely

$$\sigma_h^2 = \frac{G\, M_h}{3\, r_h} \tag{20}$$

where M_h is the mass within the radius r_h,

$$M_h = \frac{4}{3}\,\pi\, r_h^3\, \rho_h \quad , \quad Q_h = \frac{\rho_h}{\sigma_h^3} \ , \tag{21}$$

and G is Newton's gravitational constant, we obtain from eqs. (16), (20) and (21),

$$Q_h = \frac{9}{4\,\pi}\ \sqrt{\frac{3}{M_h\,(G\, r_h)^3}} \ , \tag{22}$$

and

$$r_{min} = \frac{3}{2\ \sqrt{\pi\, K}\, m^2}\left(\frac{\hbar}{\sqrt{G}}\right)^{\frac{3}{2}}\left(\frac{3\, r_h}{M_h}\right)^{\frac{1}{4}} = \frac{3\,\hbar}{2\ \sqrt{\pi\, K}}\left(\frac{m_{Pl}}{m}\right)^2\left(\frac{3\, r_h}{G\, M_h}\right)^{\frac{1}{4}} \quad , \tag{23}$$

where $m_{Pl} = \sqrt{\hbar/G}$ is Planck's mass. More explicitly

$$\frac{r_{min}}{\mathrm{pc}} = \frac{0.58793}{\sqrt{K}}\left(\frac{r_h}{\mathrm{pc}}\,\frac{10^6\ M_\odot}{M_h}\right)^{\frac{1}{4}}\left(\frac{\mathrm{keV}}{m}\right)^2 \ , \tag{24}$$

Galaxy	$\frac{r_h}{\text{pc}}$	$\frac{\sigma}{\frac{\text{km}}{\text{s}}}$	$\frac{\hbar^{\frac{3}{2}}\sqrt{Q_h}}{(\text{keV})^2}$	$\rho(0)/\frac{M_\odot}{(\text{pc})^3}$	$\frac{M_h}{10^6\ M_\odot}$
Willman 1	33	4	0.85	6.3	0.39
Segue 1	38	4	1.3	10	0.59
Leo IV	151	3.3	0.2	.19	1.14
Canis Venatici II	97	4.6	0.2	0.49	1.43
Coma-Berenices	100	4.6	0.42	2.09	1.97
Leo II	233	6.6	0.093	0.34	7.25
Leo T	152	7.8	0.12	0.79	7.4
Hercules	305	5.1	0.078	0.1	7.5
Carina	334	6.4	0.075	0.15	9.6
Ursa Major I	416	7.6	0.066	0.25	12.6
Draco	291	10.1	0.06	0.5	21
Leo I	388	9	0.048	0.22	22
Sculptor	375	9	0.05	0.25	22.5
Boötes I	322	9	0.058	0.38	24
Canis Venatici I	750	7.6	0.037	0.08	27.7
Sextans	1019	7.1	0.021	0.02	35
Ursa Minor	588	11.5	0.028	0.16	56
Fornax	944	10.7	0.016	0.053	74
NGC 185	355	31	0.033	4.09	293
NGC 855	837	58	0.01	2.64	2480
Small Spiral	4800	40.7	0.0018	0.029	5100
NGC 4478	1490	147	0.003	3.7	1.96×10^4
Medium Spiral	1.73×10^4	76.2	3.7×10^{-4}	0.0076	6.4×10^4
NGC 731	4850	163	9.27×10^{-4}	0.47	8.52×10^4
NGC 3853	4110	198	8.8×10^{-4}	0.77	8.54×10^4
NGC 499	6070	274	5.9×10^{-4}	0.91	3.27×10^5
Large Spiral	5.18×10^4	125	0.96×10^{-4}	2.3×10^{-3}	5.2×10^5

Table 2: Observed values for r_h, σ, $\sqrt{Q_h}$, $\rho(0)$ and M_h for galaxies from refs. [65, 49, 19, 24, 53, 54, 68, 9, 67, 42]. The phase space density is larger for smaller galaxies both in mass and size while the surface density $\mu = \rho(0)\ r_h$ is approximately constant [22, 30, 57, 19]. Notice that the phase space density is obtained from the stars velocity dispersion which is expected to be smaller than the DM velocity dispersion. Therefore, the reported Q_h are in fact upper bounds to the true values [53].

where we used that

$$\left(\frac{3}{2}\right)^{\frac{5}{4}} \frac{1}{\sqrt{\pi}\, 5^{\frac{1}{4}}} \frac{\hbar^{\frac{3}{2}}}{(\mathrm{kpc})^{\frac{3}{4}}\, M_{\odot}^{\frac{1}{4}}\, G^{\frac{3}{4}}\, (\mathrm{keV})^2} = 0.58793\ldots\,.$$

The values of the constant $0.60364/\sqrt{K}$ are displayed in table 1 while those of r_h/pc and $10^{-6} M_h/M_{\odot}$ are displayed in table 2.

It must be stressed that r_{min} is the **minimal** value for the core radius. The core radius can be **well above** this lower bound which corresponds to maximally packed fermions around the center of the galaxy. Hence, one expects for diluted objects as galaxies core radii much larger than the lower bound r_{min}. Even in atoms the phase-space density turns to be significantly below the quantum bound eq.(13) for thermal fermions [32]. Moreover, our derivation of r_h within the Thomas-Fermi approach presented in sec. 4 shows that $r_h \gg r_{min}$ for dwarf galaxies.

The quantum bound eq.(13) applies for any kind of fermionic dark matter. However, the value of r_{min} strongly depends on the DM particle mass.

For CDM where 1 GeV $< m <$ 100 GeV, we see that r_{min} can be from eq.(24) between dozens of kilometers and a few meters. That is, r_{min} for CDM is astronomically compatible with zero. Therefore, classical aproaches as N-body simulations and the classical Boltzmann-Vlasov equation fully apply for CDM and unavoidably produce cusps.

For HDM where 1 eV $< m <$ 10 eV, we find r_{min} from eq.(24) between the kpc and the Mpc, depending on the galaxy type. HDM suppresses all structures scales below the Mpc scale due to its long free-streaming length and has been ruled out years ago. Anyway, it is important to learn that classical aproaches to HDM as N-body simulations are not valid for scales below r_{min} which can be from the kpc to the Mpc scale according to the type of galaxy and the value of m in the eV scale.

For bosonic DM, the bound eq.(13) does not apply and the formation of cusps is allowed. However, the observed galaxy density profiles are cored [71, 61, 50, 15, 24, 65] (see also [55]).

In all cases cusps of fermionic DM in the galaxy density profile are artifacts produced by classical physics computations irrespective of the nature of dark matter (HDM, WDM, CDM) and of whether the computations are numerical or analytical.

That is, quantum physics, namely the Pauli principle, **rule out** galaxy cusps for fermionic dark matter.

We have so far ignored baryons in our analysis of the galaxies. This is fully justified for dwarf spheroidal galaxies which are composed today of 99.99% of dark matter [70, 41, 9, 67, 66]. In large galaxies the baryon fraction can reach values up to 1 - 3 % [48, 46, 43]. We have also ignored supermassive central black holes which appear in large spiral galaxies but have not been observed in dwarf galaxies. As it is known, the formation of supermassive central black holes is correlated to the formation of the galaxy itself but this whole issue is beyond the scope of the present paper. Anyway, it must be noticed that the central black hole mass is at most $\sim 10^{-3}$ of the mass of the bulge. Baryons can be important in the galaxy formation and evolution, a subject that is outside the scope of our paper. Fermionic WDM by itself produces galaxies and structures in agreement with observations. Therefore, the effect of including baryons is expected to be a correction to the pure WDM results presented in this paper, consistent with the fact that dark matter is in average six times more abundant than baryons.

2.1. Classical upper bounds from the DM phase-space density evolution

The quantum upper bound on the phase-space density eq.(13) is unrelated to the classical upper bound derived from the self-gravity classical dynamics as already noticed in ref. [59]. Namely, the fact that the coarse-grained phase-space density when averaged also in $\vec{r}$–space over a galaxy halo, can only **decrease** by classical collisionless phase mixing or classical self-gravity dynamics [28, 14, 60, 39, 40, 7, 18]. This averaged phase-space density $\overline{Q}$ is thus bounded by its primordial value Q_{prim}.

This upper bound follows from the **classical** self-gravity dynamics evolution contrary to eq.(13) which applies to fermionic DM and has a quantum origin on the Pauli principle. In addition, this classical upper bound only applies to the phase-space density averaged over a large volume and on time intervals: $\overline{Q} < Q_{prim}$.

At specific points like the galaxy center the phase-space density is classically unbounded due to the appearence of cusps and certainly much larger than the primordial phase-space density.

The primordial DM phase-space density which is space-independent can be written as [18]

$$Q_{prim} = \frac{\sqrt{27}\, g_i}{2\,\pi^2\,\hbar^3}\, m^4\, \frac{I_2^{\frac{5}{2}}}{I_4^{\frac{3}{2}}}\,, \tag{25}$$

where g_i is the number of internal degrees of freedom of the DM particle ($g_i = 4$ for Dirac fermions), I_2 and I_4 are the dimensionless momenta of the primordial DM distribution function. Using eq.(25) for Q_{prim}, its self-gravity dynamical evolution and observational data for the phase-space density today (as in Table 2) indicated that the DM particle mass is in the keV scale [18].

Inserting eq.(25) into the quantum bound eq.(13) yields

$$\sqrt{27}\, I_2^{\frac{5}{2}} \leq K\,\pi^2\, I_4^{\frac{3}{2}}\,.$$

It is easy to check that this inequality is fulfilled for the distribution functions considered in the appendix Appendix A as it must be.

That is, the primordial value Q_{prim} of the phase-space density safely fulfills the quantum bound eq.(13).

3. Gravitation and the WDM pressure: the main drivers of galaxy formation

As is well known, galaxy formation as all structure formation in the Universe is driven by gravitational physics.

The main notion regarding structure formation at a given scale r is the Jeans' length $\lambda_J(r)$ at this scale. The Jeans' length is the product of the speed of sound or the velocity of the particles v times the free fall time

$$\lambda_J(r) = v(r)\,\sqrt{\frac{\pi}{G\,\rho(r)}} \tag{26}$$

where G is Newton's gravitational constant.

Length scales larger than $\lambda_J(r)$ are gravitationally unstable. Therefore, $\lambda_J(r)$ indicates the scale of the largest objects that can be formed at the distance r. The mass density $\rho(r)$ decreases from its maximum value at the center of the galaxy $r = 0$ till asymptotic typical values 200 times the average density in the Universe at $R_{200} \sim R_{virial}$.

At a scale r structures larger than $\lambda_J(r)$ can not form because they are unstable while structures smaller than $\lambda_J(r)$ can grow reaching a size $\sim r$. Therefore,

$$r \sim \lambda_J(r) \; .$$

During the linear regime of the cosmological evolution the phase space density is small enough and the Pauli principle is always fulfilled. Notice that the phase space measure $d^3p \; d^3r$ is invariant under the universe expansion and therefore the universe expansion by itself does not affect the fullfiling of the Pauli principle.

Only when structure formation increases the particle density and particle velocity, the phase space distribution function $f(\vec{r}, \vec{p})$ may increase to approach its quantum upper bound 2 for spin one-half fermions.

In summary, starting from the linear cosmological fluctuations at WDM decoupling, we can classically evolve the phase space distribution function $f(\vec{r}, \vec{p})$ as long as f remains well below its quantum upper bound. As soon as classical physics breaks in some region, even small, we have to use a quantum mechanical treatment not only in the region where a classical f would violate the quantum upper bound but in the whole region around. This is not an easy problem and may be solved using quantum Monte Carlo methods, time dependent Hartree-Fock methods and quantum Boltzmann equations evolution [4, 5, 69, 29, 35].

Clearly, one can use the classical evolution in most of the space where f stays well below the quantum bound and match it with the quantum evolution around the galaxy centers.

The Jeans' mass is given by

$$M_J = \frac{4}{3} \, \pi \, \rho \, \lambda_J^3 = \frac{4}{3} \, \pi \, v^3 \, \sqrt{\left(\frac{\pi}{G}\right)^3 \, \frac{1}{\rho}} \; . \tag{27}$$

In terms of the phase-space density, λ_J and M_J read

$$\lambda_J = 3^{\frac{3}{4}} \, \sqrt{\frac{\pi}{G \, v \, Q}} \quad , \quad M_J = \frac{4 \, \pi^{\frac{5}{2}}}{3^{\frac{1}{4}}} \, \sqrt{\frac{v^3}{G^3 \, Q}} \; .$$

Then, from eq.(3) and eq.(4) with $\beta = 2$ we have the bound

$$\lambda_J(r) \geq \sqrt{\frac{3\,\pi}{K \, \sigma(r)}} \, \sqrt{\frac{\hbar}{G}} \, \frac{\hbar}{m^2} \; , \tag{28}$$

More explicitly, we get a lower bound of the product of the Jeans' length and the square root of the velocity dispersion

$$\sqrt{\sigma(r)} \;\; \lambda_J(r) \geq \frac{0.339}{\sqrt{K}} \, \left(\frac{\text{keV}}{m}\right)^2 \;\; \text{pc}$$

showing that neither the Jeans' length nor the velocity dispersion can vanish for $r \to 0$.

3.1. Dwarf galaxies as WDM quantum macroscopic objects

To determine whether a system of particles has a classical or quantum nature we should compare the particle de Broglie wavelength with the interparticle distance.

The de Broglie wavelength of DM particles in a galaxy can be estimated as

$$\lambda_{dB} = \frac{\hbar}{m\,\sigma}\ , \tag{29}$$

while the average interparticle distance d can be estimated as

$$d = \left(\frac{m}{\rho_h}\right)^{\frac{1}{3}}\ , \tag{30}$$

where ρ_h is the average density in the galaxy core. By using $\rho_h = \sigma^3\ Q_h$ and eqs.(29)-(30), we can express the ratio

$$\mathcal{R} \equiv \frac{\lambda_{dB}}{d}$$

as,

$$\mathcal{R} = \hbar\ \left(\frac{Q_h}{m^4}\right)^{\frac{1}{3}}\ . \tag{31}$$

Using now the observed values of Q_h from Table 2 yields

$$2\times 10^{-3} < \mathcal{R}\ \left(\frac{m}{\text{keV}}\right)^{\frac{4}{3}} < 1.4 \tag{32}$$

The larger value of $\mathcal{R}$ is for ultracompact dwarfs and the smaller value of $\mathcal{R}$ is for big spirals.

The ratio $\mathcal{R}$ around unity clearly implies a macroscopic quantum object.

Notice that here as well as in the bound eq.(13) $\hbar^3\ Q/m^4$ measures how quantum or classical is the system (the galaxy).

We conclude **solely from observations** that compact dwarf galaxies are natural macroscopic quantum objects for WDM.

3.2. Dwarf Galaxies supported by WDM fermionic quantum pressure

For an order–of–magnitude estimate, let us consider a halo of mass M and radius R of fermionic matter. It can be fermionic DM or baryons. Each fermion can be considered inside a cell of size $\Delta x \sim 1/n^{\frac{1}{3}}$ and therefore has a momentum

$$p \sim \frac{\hbar}{\Delta x} \sim \hbar\, n^{\frac{1}{3}}\ .$$

The associated quantum pressure P_q (flux of the momentum) has the value

$$P_q = n\,\sigma\ p \sim \hbar\,\sigma\, n^{\frac{4}{3}} = \frac{\hbar^2}{m}\ n^{\frac{5}{3}}\ . \tag{33}$$

where σ is the mean velocity given by

$$\sigma = \frac{p}{m} = \frac{\hbar}{m}\ n^{\frac{1}{3}}\ .$$

The system will be in dynamical equilibrium if this quantum pressure is balanced by the gravitational pressure

$$P_G = \text{gravitational force/area} = \frac{G\,M^2}{R^2} \times \frac{1}{4\,\pi\,R^2} \tag{34}$$

We estimate the number density as

$$n = \frac{M}{\frac{4}{3}\,\pi\,R^3\,m}\ ,$$

and we use that $p = m\,\sigma$ to obtain from eq.(33)

$$P_q = \frac{\hbar^2}{m\,R^5}\,\left(\frac{3\,M}{4\,\pi\,m}\right)^{\frac{5}{3}}\ . \tag{35}$$

Equating $P_q = P_G$ from eqs.(34)-(35) yields the following relations between the size R and the velocity σ with the mass M of the system:

$$R = \frac{3^{\frac{5}{3}}}{(4\,\pi)^{\frac{2}{3}}}\,\frac{\hbar^2}{G\,m^{\frac{8}{3}}\,M^{\frac{1}{3}}} = 10.6\ldots\,\text{pc}\,\left(\frac{10^6\,M_\odot}{M}\right)^{\frac{1}{3}}\,\left(\frac{\text{keV}}{m}\right)^{\frac{8}{3}} \tag{36}$$

$$\sigma = \left(\frac{4\,\pi}{81}\right)^{\frac{1}{3}}\,\frac{G}{\hbar}\,m^{\frac{4}{3}}\,M^{\frac{2}{3}} = 22.9\ldots\,\frac{\text{km}}{\text{s}}\,\left(\frac{m}{\text{keV}}\right)^{\frac{4}{3}}\,\left(\frac{M}{10^6\,M_\odot}\right)^{\frac{2}{3}}\ . \tag{37}$$

Notice that the values of M, R and σ are consistent with dwarf galaxies. Namely, for M of the order $10^6\ M_\odot$ (typical mass value for dwarf spheroidal galaxies), R and σ have the correct order of magnitude for dwarf spheroidal galaxies for a WDM particles mass in the keV scale (see Table 2).

These results back the idea that dwarf spheroidal galaxies are supported by the fermionic *WDM quantum pressure* eq.(35).

It is useful to express the above quantities in terms of the density ρ, as follows

$$M = \frac{9\,\hbar^3}{2\,m^4}\,\sqrt{\frac{\rho}{\pi\,G}} = 0.7073\ldots 10^5\,M_\odot\,\sqrt{\rho\,\frac{\text{pc}^3}{M_\odot}}\,\left(\frac{\text{keV}}{m}\right)^4\ , \tag{38}$$

$$R = \frac{3\,\hbar}{2\,\sqrt{\pi\,G}}\,\frac{1}{m^{\frac{4}{3}}\,\rho^{\frac{1}{6}}} = 31.05\ldots\ \text{pc}\,\left(\frac{M_\odot}{\rho\ \text{pc}^3}\right)^{\frac{1}{6}}\,\left(\frac{\text{keV}}{m}\right)^{\frac{4}{3}}\ ,$$

$$\sigma = \hbar\,\left(\frac{\rho}{m^4}\right)^{\frac{1}{3}} = 1.990\ldots\,\frac{\text{km}}{\text{s}}\,\left(\rho\,\frac{\text{pc}^3}{M_\odot}\right)^{\frac{1}{3}}\,\left(\frac{\text{keV}}{m}\right)^{\frac{4}{3}}\ , \tag{39}$$

$$P_q = \hbar^2\,\frac{\rho^{\frac{5}{3}}}{m^{\frac{8}{3}}} = 4.399\ 10^{-11}\,\frac{M_\odot}{\text{pc}^3}\,\left(\rho\,\frac{\text{pc}^3}{M_\odot}\right)^{\frac{5}{3}}\,\left(\frac{\text{keV}}{m}\right)^{\frac{8}{3}}\ , \tag{40}$$

R and M are typical *semiclassical gravitational* quantities involving both G and $\hbar$. The particle velocity σ and the pressure P_q are of purely quantum mechanical origin.

The radius R and mass M are the *semiclassical* Jeans' length and Jeans' mass as can be seen by inserting the velocity from eq.(39) in eqs.(26) and (27) with the result

$$\lambda_J = \frac{2\,\pi}{3}\,R \quad , \quad M_J = \left(\frac{2\,\pi}{3}\right)^3\,M$$

The associated phase-space density results

$$Q = \frac{m^4}{\hbar^3} \ .$$

In this case where v has purely quantum origin [eq.(39)], the de Broglie wavelength is equal to the interparticle distance $\lambda_{dB} = d$. Thus the ratio $\mathcal{R}$ is unity which is the extreme (fermion degenerate) quantum case.

In the presence of squared angular momentum L^2 we have to add the centrifugal pressure

$$P_L = \frac{1}{4\,\pi\,R^2}\ \frac{L^2}{M\,R^3}$$

in the equilibration equation $P_q + P_L = P_G$. The relation between the radius, mass and velocity eq.(36) takes now the form

$$R = \frac{L^2}{G\,M^3} + \frac{3^{\frac{5}{3}}}{(4\,\pi)^{\frac{2}{3}}}\ \frac{\hbar^2}{G\,m^{\frac{8}{3}}\,M^{\frac{1}{3}}} \ . \tag{41}$$

A simple estimation of the total angular momentum of the whole halo goes as follows

$$L^2 \sim \frac{1}{2}\ M^2\,R^2\,3\,\sigma^2$$

where the $\frac{1}{2}$ factor comes from averaging the $\sin^2$ of the angle between the momentum $\vec{p}$ and the particle position $\vec{r}$, and the factor 3 comes from the relation $v^2 = 3\,\sigma^2$. We thus obtain

$$R = 10.6\ldots\mathrm{pc}\left(\frac{10^6\,M_\odot}{M}\right)^{\frac{1}{3}}\left(\frac{\mathrm{keV}}{m}\right)^{\frac{8}{3}} + 3.48\ldots\mathrm{pc}\ \frac{10^6\,M_\odot}{M}\left(\frac{\sigma}{10\ \frac{\mathrm{km}}{\mathrm{s}}}\ \frac{R}{10\ \mathrm{pc}}\right)^2 \ . \tag{42}$$

We see that the angular momentum contribution increases the size R. However, for dwarf galaxies, we see that R and σ have the same order of magnitude for $L > 0$ and for $L = 0$.

4. Galaxy properties from quantum fermionic WDM in the Thomas-Fermi approach

DM particles are nonrelativistic during structure formation and their chemical potential is given by

$$\mu(r) = \mu_0 - m\,\phi(r) \tag{43}$$

where m is the mass of the DM particle, μ_0 is a constant and $\phi(r)$ is the gravitational potential.

We consider for simplicity the spherical symmetric case where the Poisson equation for the gravitational potential takes the form

$$\frac{d^2\mu}{dr^2} + \frac{2}{r}\ \frac{d\mu}{dr} = -4\,\pi\,G\,m\,\rho(r) \tag{44}$$

where G is Newton's gravitational constant and $\rho(r)$ is the DM mass density.

Since the DM mass density is bounded by the Pauli principle as analyzed in sec. 2, $\rho(r)$ must be bounded at the origin and therefore we must impose as boundary condition at the origin:

$$\frac{d\mu}{dr}(0) = 0 \ . \tag{45}$$

We can write the DM mass density as the integral over the momentum of the DM distribution function

$$\rho(r) = \frac{g\ m}{2\ \pi^2\ \hbar^3} \int_0^\infty p^2\ dp\ f[e(p) - \mu(r)] \tag{46}$$

where $e(p) = p^2/(2\,m)$ is the particle kinetic energy, $f(E)$ is the energy distribution function and g is the number of internal degrees of freedom of the DM particle. $g = 1$ for Majorana fermions and $g = 2$ for Dirac fermions.

Eqs.(44) and (46) provide a system of ordinary nonlinear differential equations that determine the chemical potential $\mu(r)$ and constitutes the Thomas-Fermi semi-classical approximation. Fermionic DM in the Thomas-Fermi approximation has been previously considered in ref. [3, 10, 11, 44].

The Thomas-Fermi equations provide a semi-classical approximation in which the energy distribution function $f(E)$ is given.

The boundary condition for the chemical potential is usually set to zero at a given radius R which is the appropriate condition for the Coulomb interaction in atoms [32] and for self-gravitating degenerate fermions [31]. In the selfgravitating degenerate case the mass density is proportional to the power $3/2$ of the chemical potential and therefore both quantities vanish at the same point. In the general selfgravitating case for non-degenerate fermions where eq.(46) applies, the mass density stays nonzero beyond the point where the chemical potential changes sign and becomes negative.

We integrate the Thomas-Fermi nonlinear differential equations (44)-(46) from $r = 0$ till the boundary $r = R = R_{200} \sim R_{vir}$ defined as the radius where the mass density equals 200 times the mean DM density.

In order to determine the distribution function $f(E)$ one should follow the precise DM evolution since decoupling. Such evolution must take into account the quantum character that emerges when the distribution function approaches the quantum upper bound eq.(3). This quantum dynamical calculation is beyond the scope of the present paper.

We modelize here the distribution function $f(E)$ by equilibrium Fermi-Dirac functions and by out of equilibrium Dodelson-Widrow and ν-MSM distribution functions (see the appendix Appendix A).

Let us define dimensionless variables $\nu(\xi)$, ξ, ξ_0 and the dimensionless distribution function Ψ as

$$r = L_0\ \xi \qquad , \qquad R = L_0\ \xi_0 \qquad , \qquad \mu(r) = E_0\ \nu(\xi) \qquad , \qquad f(E) = \Psi\left[\frac{E}{E_0}\right] , \tag{47}$$

where E_0 is the characteristic comoving energy of the DM particles at decoupling. The characteristic length L_0 emerges from the dynamical equations (44)-(46) and is given by

$$L_0 \equiv \frac{\sqrt{3\,\pi\ \hbar^3}}{\sqrt{G}\ (2\,m)^2} \left(\frac{2\,m}{E_0}\right)^{\frac{1}{4}} , \tag{48}$$

For $g = 2$ the mass density takes the form

$$\rho(r) = \frac{m^4}{\pi^2\,\hbar^3}\left(\frac{2\,E_0}{m}\right)^{\frac{3}{2}}\beta(\nu(\xi)) \quad , \quad \beta(\nu) \equiv \int_0^\infty y^2\,dy\,\Psi(y^2-\nu)\,, \tag{49}$$

where we use the integration variable $y \equiv p/\sqrt{2\,m\,E_0}$ and the Poisson equation (44)-(46) become

$$\frac{d^2\nu}{d\xi^2} + \frac{2}{\xi}\,\frac{d\nu}{d\xi} = -3\,\beta(\nu(\xi)) \quad , \quad \rho(\xi_0) = 200\,\bar{\rho}_{DM} \quad , \quad \nu'(0) = 0 \quad , \tag{50}$$

The distribution functions Ψ are given in the Appendix Appendix A for the thermal and out of equilibrium cases.

In order to integrate eq.(50) we have to specify $\nu(0)$. $\nu(0)$ is determined by the value of the phase space density at the origin $Q(r=0)$. That is, to find a given galaxy we must give $Q(r=0)$ and the boundary radius R in dimensionless variables ξ_0. In eq.(66) below we find the relation between $\nu(0)$ and $Q(r=0)$ which permits to compute $\nu(0)$ from a given value of $Q(r=0)$.

4.1. Main physical galaxy properties: mass, velocity dispersion, density and pressure

We derive in this subsection the expressions for the main physical properties of the galaxies (mass, velocity dispersion, density and pressure) in the Thomas-Fermi semi-classical approximation.

The average velocity of the particles is space-dependent and follows from the average momentum given by

$$v^2(r) = \frac{1}{m^2}\,\frac{\int_0^\infty p^4\,dp\;f[e(p)-\mu(r)]}{\int_0^\infty p^2\,dp\;f[e(p)-\mu(r)]} = \frac{2\,E_0}{m}\,\alpha^2(\nu(\xi))\,, \tag{51}$$

where

$$\alpha(\nu) \equiv \sqrt{\frac{\int_0^\infty y^4\,dy\,\Psi(y^2-\nu)}{\int_0^\infty y^2\,dy\,\Psi(y^2-\nu)}}\,. \tag{52}$$

The mass enclosed in the sphere of radius R follows by integrating the mass density given by eq.(49)

$$M = 4\,\pi\int_0^R r^2\,dr\,\rho(r) = \frac{\sqrt{27\,\pi}}{2\,m^2}\left(\frac{\hbar}{G}\right)^{\frac{3}{2}}\left(\frac{E_0}{2\,m}\right)^{\frac{3}{4}}\int_0^{\xi_0}\xi^2\,d\xi\,\beta(\nu(\xi))\,, \tag{53}$$

where we used eqs.(47) and (48). The integral over ξ can be performed with the help of eq.(50),

$$\int_0^{\xi_0}\xi^2\,d\xi\,\beta(\nu(\xi)) = -\frac{1}{3}\,\xi_0^2\,\nu'(\xi_0)\,. \tag{54}$$

Notice that $\nu'(\xi_0)$ is always negative since the function $\beta(\nu)$ is positive definite.

We can write from eqs.(53)-(54) the mass M as

$$M = \frac{\sqrt{3\,\pi}}{2\,m^2}\left(\frac{\hbar}{G}\right)^{\frac{3}{2}}\left(\frac{E_0}{2\,m}\right)^{\frac{3}{4}}\xi_0^2\,\left|\nu'(\xi_0)\right|\,. \tag{55}$$

The pressure at the point r, $P(r)$ is given by an analogous integral [7]

$$P(r) = \frac{m^4}{3\,\pi^2\,\hbar^3}\,\left(\frac{2\,E_0}{m}\right)^{\frac{5}{2}}\,\int_0^\infty y^4\,dy\,\Psi[y^2-\nu(\xi)] = \frac{m^4}{3\,\pi^2\,\hbar^3}\,\left(\frac{2\,E_0}{m}\right)^{\frac{5}{2}}\,\alpha^2(\nu(\xi))\,\beta(\nu(\xi))\;. \quad (56)$$

From eqs.(49) and (51) we can write the density and the average square velocity as

$$\rho(r) = \rho(0)\,\frac{\beta(\nu(\xi))}{\beta_0} \quad , \quad v(r) = v(0)\,\frac{\alpha(\nu(\xi))}{\alpha_0}\;,$$

Here $\alpha_0 \equiv \alpha(\nu(0))$ and $\beta_0 \equiv \beta(\nu(0))$.

Moreover, from eqs.(49), (51) and (56) we derive as local equation of state:

$$P(r) = \frac{1}{3}\,v^2(r)\,\rho(r)\;\;. \quad (57)$$

This local equation of state generalizes the local perfect fluid equation of state for r-dependent velocity $v(r)$. As we see below, the perfect fluid equation of state is recovered both in the classical dilute limit and in the quantum degenerate limit.

It is very instructive to compute the derivative of the pressure eq.(56) with respect to $r = L_0\,\xi$. Upon integrating by parts and using eqs.(43), (47) and (49) we find

$$\frac{dP}{dr} + \rho(r)\,\frac{d\phi}{dr} = 0\;. \quad (58)$$

This shows that the quantum Thomas-Fermi equation implies the hydrostatic equilibrium equation.

By analogy with the Burkert density profile, the halo radius $r_h = L_0\;\xi_h$ in this theoretical calculation can be defined in dimensionless variables as,

$$\frac{\rho(r_h)}{\rho(0)} = \frac{\beta(\xi_h)}{\beta_0} = \frac{1}{4}\;.$$

Furthermore, from eqs.(49) and (51) the phase space density $Q(r)$ is given by

$$Q(r) = \frac{\sqrt{27}}{\pi^2\,\hbar^3}\;\;m^4\;\;\frac{\beta(\xi)}{\alpha^3(\xi)} \quad \text{and} \quad Q(0) = \frac{\sqrt{27}}{\pi^2\,\hbar^3}\;\;m^4\;\;\frac{\beta_0}{\alpha_0^3}\;, \quad (59)$$

which turns to be independent of E_0.

From eqs.(47), (48) and (55), $R^3\;M$ turns to be independent of E_0 too:

$$R^3\;M = \frac{(3\,\pi)^2\;\hbar^6}{G^3\;(2\,m)^8}\;\;\xi_0^5\;\;\left|\nu'(\xi_0)\right|\;.$$

We expressed above the main physical galaxy magnitudes L_0, M, $v(r)$, $P(r)$ and $\rho(r)$ in terms of the DM characteristic energy E_0 and the potential $\nu(\xi)$, solution of eq.(50). Because E_0 is not directly observed we will eliminate E_0 in terms of $\rho(r=0)$ from eq.(49). [We may also choose other point $r \neq 0$]. We obtain

$$\left(\frac{2\,E_0}{m}\right)^{\frac{3}{2}} = \frac{\pi^2\;\hbar^3}{m^4}\;\frac{\rho(0)}{\beta_0}\;. \quad (60)$$

By eliminating E_0 and using eqs.(49)-(52), we have for the pressure eq.(56)

$$P(r) = \frac{\pi^{\frac{4}{3}}}{3}\,\hbar^2\,m^4\,\left[\frac{\rho(0)}{\beta_0\,m^4}\right]^{\frac{5}{3}}\,\alpha^2(\nu)\,\beta(\nu) \quad \text{and} \quad P(0) = \frac{\pi^{\frac{4}{3}}}{3}\,\hbar^2\,m^4\,\left[\frac{\rho(0)}{m^4}\right]^{\frac{5}{3}}\,\left(\frac{\alpha_0}{\beta_0^{\frac{1}{3}}}\right)^2 \,. \tag{61}$$

Inserting eq.(60) in eqs.(47), (48), (51) and (55) yields

$$L_0 = \sqrt{\frac{3}{8\,G}}\,\frac{\hbar}{m^{\frac{4}{3}}}\,\left[\frac{\pi\,\beta_0}{\rho(0)}\right]^{\frac{1}{6}} \quad , \quad \nu(r) = \hbar\,\alpha(\nu)\,\left[\frac{\pi^2\,\rho(0)}{\beta_0\,m^4}\right]^{\frac{1}{3}} \quad , \quad M = \frac{\sqrt{3}\,\pi^{\frac{3}{2}}\,\hbar^3}{2^{\frac{5}{2}}\,G^{\frac{3}{2}}\,m^2}\;\;\xi_0^2\;\left|\nu'(\xi_0)\right|\,\sqrt{\frac{\rho(0)}{\beta_0\,m^4}}\,. \tag{62}$$

More explicitly, we can express L_0, M and $\nu(r)$ as

$$L_0 = R_0\;\left(\frac{\text{keV}}{m}\right)^{\frac{4}{3}}\,\left[\frac{\beta_0\,M_\odot}{\rho(0)\;\text{pc}^3}\right]^{\frac{1}{6}} \quad , \quad R_0 \equiv \sqrt{\frac{3}{8\,G}}\,\frac{\hbar}{\text{keV}^{\frac{4}{3}}}\,\left[\frac{\pi\;\text{pc}^3}{M_\odot}\right]^{\frac{1}{6}} = 22.47\;\text{pc}\,, \tag{63}$$

$$M = M_0\;\sqrt{\rho(0)\,\frac{\text{pc}^3}{M_\odot}}\;\left(\frac{\text{keV}}{m}\right)^4\;\frac{\xi_0^2}{\sqrt{\beta_0}}\;\left|\nu'(\xi_0)\right| \quad , \quad M_0 \equiv \frac{\sqrt{3}\,\pi^{\frac{3}{2}}\,\hbar^3}{2^{\frac{5}{2}}\,G^{\frac{3}{2}}\;\text{keV}^4}\;\sqrt{\frac{M_\odot}{\text{pc}^3}} = 1.425\;10^5\;M_\odot\,,$$

$$\nu(r) = \nu_0\;\left[\rho(0)\,\frac{\text{pc}^3}{M_\odot}\right]^{\frac{1}{3}}\,\left(\frac{\text{keV}}{m}\right)^{\frac{4}{3}}\;\frac{\alpha(\nu)}{\beta_0^{\frac{1}{3}}} \quad , \quad \nu_0 \equiv \pi^{\frac{2}{3}}\,\left[\frac{M_\odot}{\text{pc}^3}/\text{keV}^4\right]^{\frac{1}{3}} = 4.268\;\;\frac{\text{km}}{\text{s}}\,. \tag{64}$$

The *semiclassical* galaxy magnitudes L_0, M, $\nu(0)$ and $P(0)$ emerging from the Thomas-Fermi equations generalize the corresponding expressions eq.(38)-(39) derived just equating the gravitational and WDM quantum pressures and describing the quantum degenerate fermions limit. Eqs.(63)-(64) cover the full range of physical situations from the degenerate fermions till the dilute classical limit as we discuss in the next subsection.

The local Jeans' length and Jeans' mass follow by inserting eqs.(49) and (51) for $\rho(r)$ and $\nu(r)$, respectively, into eqs.(26) and (27)

$$\lambda_J(\xi) = \pi\;\sqrt{\frac{8}{3}}\,L_0\,\frac{\alpha(\xi)}{\sqrt{\beta(\xi)}} \quad , \quad M_J(\xi) = \frac{8\,\pi^3}{\sqrt{27}}\;\;M\;\;\frac{\alpha^3(\xi)}{\sqrt{\beta(\xi)}}\frac{1}{\xi_0^2}\;\left|\nu'(\xi_0)\right| \tag{65}$$

We see that λ_J and M_J differ from $L_0 = R/\xi_0$ and M by ξ-dependent factors of order one. Therefore, the galaxy length scale L_0 and galaxy mass M emerging from the Thomas-Fermi equation (50) are a measure of the Jeans' length λ_J and the Jeans' mass M_J, respectively.

From eqs.(49), (52) and using $Q(0) = 3\;\sqrt{3}\,\rho(0)/\nu^3(0)$, eq.(64) can be rewritten as

$$\frac{\alpha_0}{\beta_0^{\frac{1}{3}}} = \frac{\left\{\int_0^\infty y^4\;dy\;\Psi[y^2-\nu(0)]\right\}^{\frac{1}{2}}}{\left\{\int_0^\infty y^2\;dy\;\Psi[y^2-\nu(0)]\right\}^{\frac{5}{6}}} = \frac{2.145\ldots}{\hbar}\,\left[\frac{\text{keV}^4}{Q(0)}\right]^{\frac{1}{3}}\,\left(\frac{m}{\text{keV}}\right)^{\frac{4}{3}} = 1.0772\,\left[\frac{M_\odot}{Q(0)\;\text{pc}^3\;\left(\frac{\text{km}}{\text{s}}\right)^3}\right]^{\frac{1}{3}}\,\left(\frac{m}{\text{keV}}\right)^{\frac{4}{3}}\,. \tag{66}$$

Eq.(66) shows that $\nu(0)$ is determined by the phase density at the origin $Q(0)$. In the next subsection we solve the Thomas-Fermi eqs.(50) in the whole range of the chemical potential at the origin $\nu(0)$.

4.2. Physical galaxy properties from the resolution of the Thomas-Fermi equation

Large positive values of the chemical potential at the origin $\nu(0) \gg 1$ correspond to the degenerate fermions limit which is the extreme quantum case and oppositely, $\nu(0) \ll -1$ gives the diluted limit. The diluted limit is the classical limit and in this case the Thomas-Fermi equations (44)-(46) become the equations for a selfgravitating Boltzmann gas.

The bounds on the phase space density follows from eqs.(49), (52) and (59),

$$0 < \hbar^3 \, \frac{Q(0)}{m^4} \leq \frac{5\,\sqrt{5}}{3\,\pi^2} = 0.37760\ldots \quad \text{and} \quad 0 < \hbar^{\frac{3}{2}} \, \frac{\sqrt{Q(0)}}{m^2} \leq 0.61449\ldots \quad \text{for} \quad -\infty < \nu(0) \leq \infty \tag{67}$$

The largest value for the phase space density corresponds to the degenerate fermions limit while the smallest values appear in the classical dilute limit.

In the quantum degenerate fermions limit, the halo radius, the velocity dispersion and the galaxy mass take their *minimum* values:

$$\begin{aligned} r_{h\,min} &= 24.516\ \text{pc} \left(\frac{\text{keV}}{m}\right)^{\frac{4}{3}} \left[\rho(0)\,\frac{\text{pc}^3}{M_\odot}\right]^{\frac{1}{6}} \quad , \\ M_{min} &= 1.291\ 10^5\ M_\odot \left(\frac{\text{keV}}{m}\right)^4 \sqrt{\frac{\rho(0)\ \text{pc}^3}{M_\odot}} \quad , \\ v_{min}(0) &= 4.768\ \frac{\text{km}}{\text{s}} \left(\frac{\text{keV}}{m}\right)^{\frac{4}{3}} \left[\frac{\rho(0)\ \text{pc}^3}{M_\odot}\right]^{\frac{1}{3}} \quad . \end{aligned} \tag{68}$$

These minimum values are similar to the estimates for degenerate fermions eqs.(38)-(39), as it must be.

The masses of compact dwarf spheroidal galaxies dominated by DM must be larger than the minimum mass M_{min} eq.(68). The lightest known galaxy of this kind is Willman I (see Table 2). Imposing $M_{min} < M_{Willman\ I} = 3.9\ 10^5\ M_\odot$ gives a lower bound for the WDM particle mass:

$$m > 0.96\ \text{keV} \ . \tag{69}$$

Approaching the classical diluted limit yields larger and larger halo radii, galaxy masses and velocity dispersions. Their maximum values are limited by the initial conditions provided by the primordial power spectrum which determines the sizes and masses of the galaxies formed.

The phase space density decreases from its maximum value for the compact dwarf galaxies corresponding to the degenerate fermions limit till its smallest value for large galaxies (spirals and ellipticals) corresponding to the classical dilute regime.

Thus, the whole range of values of the chemical potential at the origin $\nu(0)$, given by the boundary condition, from the extreme quantum (degenerate) limit $\nu(0) \gg 1$ to the classical (Boltzmann) dilute regime $\nu(0) \ll -1$ yield all masses, sizes, phase space densities and velocities of galaxies from the ultra compact dwarfs till the larger spirals and elliptical in agreement with the observations (see Table 2).

In the degenerate limit the equilibrium FD thermal case and the out of equilibrium case give identical results, as expected.

In fig. 1 we plot from eq.(59) the dimensionless quantity

$$\frac{\hbar^{\frac{3}{2}}\ \sqrt{Q(0)}}{m^2} = \frac{3^{\frac{3}{4}}}{\pi}\ \frac{\beta_0}{\alpha_0^3}\ . \tag{70}$$

In fig. 2, we plot the dimensionless product

$$\frac{M}{M_\odot}\sqrt{\frac{M_\odot}{\rho(0)\ \mathrm{pc}^3}}\ \left(\frac{m}{\mathrm{keV}}\right)^4 = 1.425\ 10^5\ \frac{\xi_0^2}{\sqrt{\beta_0}}\ \ \left|\nu'(\xi_0)\right|\ , \tag{71}$$

where M is the galaxy mass and we used eqs.(63)-(64). In both figures we plot in the abscissa the product

$$r_h\ \left(\frac{m}{\mathrm{keV}}\right)^{\frac{4}{3}}\ \left[\frac{\mathrm{pc}^3}{M_\odot}\ \rho(0)\right]^{\frac{1}{6}} = R_0\ \beta_0^{\frac{1}{6}}\ \xi_h \quad \text{in parsecs,} \tag{72}$$

where r_h is the halo radius. The phase-space density $Q(0)$ and the galaxy mass M are obtained by solving the Thomas-Fermi eqs.(50) for thermal (FD) fermions and for out of equilibrium sterile neutrinos with the distribution eq.(A.6).

Notice that the theoretical curves in the right-hand side of eqs.(70)-(72) are independent of the value m of the DM particle and do not change with m.

In fig. 1 we have superimposed the observed values of $\sqrt{Q_h}/m^2$ for $m = 1$ keV, $m = 2$ keV and $m = 5$ keV (see Table 2). Notice that the observed values of Q_h from the stars' velocity dispersion are in fact upper bounds for the DM Q_h. This may explain why the theoretical Thomas-Fermi curves in fig. 1 appears below the observational data. Notice that the error bars of the observational data are not reported here but they are at least about $10 - 20\%$.

In fig. 2 we have superimposed the observed values of $(M/M_\odot)\sqrt{M_\odot/[\rho(0)\ \mathrm{pc}^3]}\ \ (m/\mathrm{keV})^4$ for $m = 1$ keV, $m = 2$ keV and $m = 5$ keV (see Table 2).

We see from fig. 1 that increasing the DM particle value just pushes down and to the right the observed values $\hbar^{\frac{3}{2}}\ \sqrt{Q_h}/m^2$. In fig. 2 we see that increasing the DM particle value just pushes up and to the right the observed values $(M/M_\odot)\sqrt{M_\odot/[\rho(0)\ \mathrm{pc}^3]}\ \ (m/\mathrm{keV})^4$.

As noticed above from eqs.(70)-(72), the theoretical curves are independent of the value m of the DM particle. Hence, for growing $m \gtrsim$ keV the left part of the theoretical curves will have no observed galaxy counterpart. Namely, increasing $m \gg$ keV shows an overabundance of small galaxies (small scale structures) without observable counterpart. This is a further indication that the WDM particle mass is approximately in the range 1 - 2 keV.

The galaxy velocity dispersions from eq.(64) turn to be fully consistent with the galaxy observations in Table 2.

We see in figs. 1 and 2 that fermions at equilibrium and out of equilibrium give very similar values for $Q(0)$ and M. The theoretical values for r_h, M and $v(0)$ vary very little with the distribution function Ψ. This is similar to the WDM linear power spectrum [20], where changing the distribution function can be balanced by changing the mass m within the keV scale.

Notice that the values obtained for the halo radius r_h in fig. 1 are much larger than the quantum lower bound r_{min} eq.(19), as expected.

In summary, the theoretical Thomas-Fermi results are fully consistent with all the observations especially for dwarf compact galaxies as can be seen from Table 2. This result gives an

additional support to the idea put forward in sec. 3.2 that galaxies are supported against gravity by the fermionic WDM quantum pressure.

It is highly remarkably that in the context of fermionic WDM the simple static quantum description provided by Thomas-Fermi is able to reproduce such broad variety of galaxies.

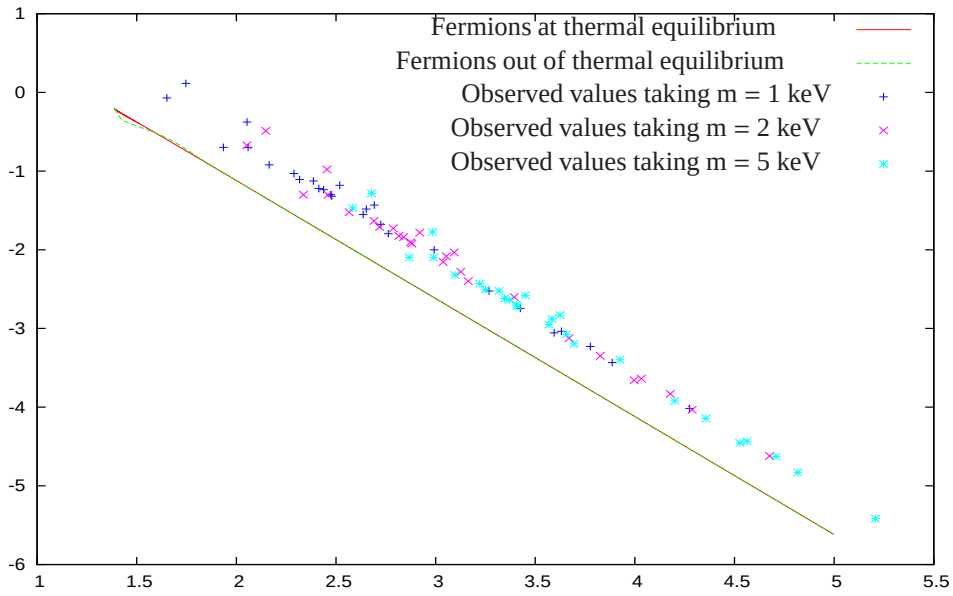

Figure 1: The ordinary logarithm of the square root of the galaxy phase-space density $\log_{10}[\hbar^{\frac{3}{2}}\ \sqrt{Q(0)}/m^2] = \log_{10}[3^{\frac{3}{4}}\ \ \beta_0/(\pi\ \ \alpha_0^3)]$ defined in eq.(59) as a function of the ordinary logarithm of the product $\log_{10}\{r_h\ (m/\text{kev})^{\frac{4}{3}}\ [\text{pc}^3\ \rho(0)/M_\odot]^{\frac{1}{6}}\} = \log_{10}[R_0\ \beta_0^{\frac{1}{6}}\ \xi_h]$ in parsecs from the numerical resolution of the Thomas-Fermi eqs.(50) for WDM fermions. The red (solid) curve is for thermal fermions and the green (dashed) curve corresponds to out of equilibrium sterile neutrinos with the distribution eq.(A.6). The blue crosses + are the observed values of $\hbar^{\frac{3}{2}}\ \sqrt{Q(0)}/m^2$ from Table 2 for $m = 1$ keV, the red X are the observed values for $m = 2$ keV and the light blue stars are the observed values for $m = 5$ keV. Notice that the observed Q_h from the stars' velocity dispersion are in fact upper bounds for the DM Q_h.

To conclude, eqs.(63) indicate that the galaxy magnitudes (halo radius, galaxy masses and velocity dispersion) obtained from the Thomas-Fermi quantum treatment for fermion masses in the keV scale are fully consistent with all the observations especially for compact dwarfs (see Table 2). Namely, fermionic WDM treated quantum mechanically (as it must be) is able to reproduce the observed sizes of the DM cores of galaxies.

acknowledgments

We are grateful to Peter Biermann for useful discussions in many occasions. We thank Daniel Boyanovsky for useful remarks.

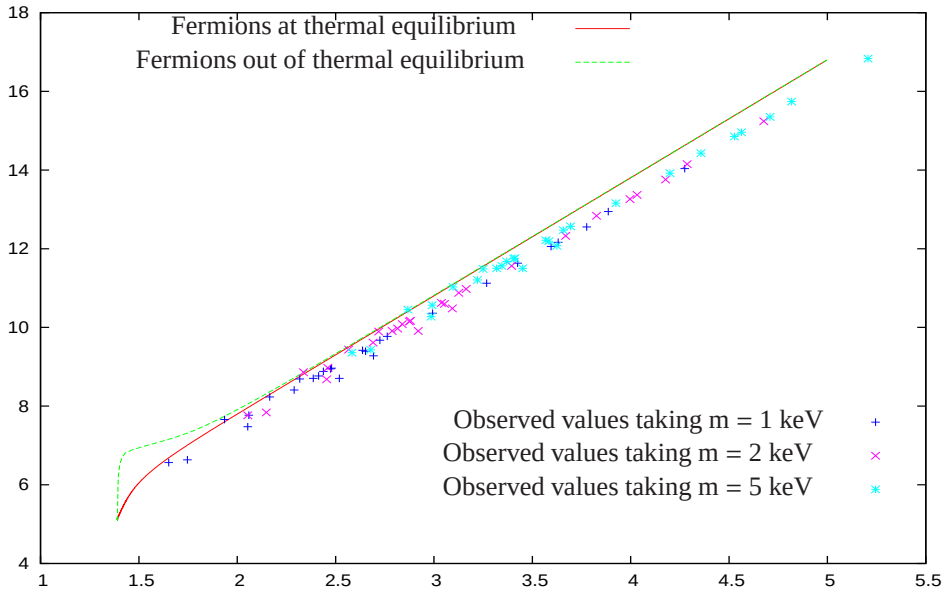

Figure 2: The ordinary logarithm of the galaxy mass $\log_{10}[(M/M_\odot)\sqrt{M_\odot/[\rho(0)\ \mathrm{pc}^3]}\quad (m/\mathrm{keV})^4] = \log_{10}[1.425\quad 10^5\quad \xi_0^2\quad |\nu'(\xi_0)|\,/\,\sqrt{\beta_0}]$ as a function of the ordinary logarithm of the product $\log_{10}\{r_h\ (m/\mathrm{kev})^{\frac{4}{3}}\ [\mathrm{pc}^3\ \rho(0)/M_\odot]^{\frac{1}{6}}\} = \log_{10}[R_0\ \beta_0^{\frac{1}{6}}\ \xi_h]$ in parsecs from the numerical resolution of the Thomas-Fermi eqs.(50) for WDM fermions. The red (solid) curve is for thermal fermions and the green (dashed) curve corresponds to out of equilibrium sterile neutrinos with the distribution eq.(A.6). The blue crosses + are the observed values of $\log_{10}[(M/M_\odot)\sqrt{M_\odot/[\rho(0)\ \mathrm{pc}^3]}\quad (m/\mathrm{keV})^4]$ from Table 2 for $m = 1$ keV, the red X are the observed values for $m = 2$ keV and the light blue stars are the observed values for $m = 5$ keV.

Appendix A. Halo bounds from the Pauli Principle

We derive here bounds on the phase space density $Q(r)$ from the Pauli Principle assuming a simple factorized form for the phase space distribution function

$$f(\vec{r},\vec{p}) = n(\vec{r})\ \Psi(p/p_0)\ ,$$

where p_0 is the momentum characteristic scale of the DM particles. For fermions at thermal equilibrium p_0 coincides with the temperature. Since the DM number density follows integrating $f(\vec{r},\vec{p})$ over $\vec{p}$ as in eq.(10), the function $\Psi(p/p_0)$ must fulfill

$$1 = \int d^3p\ \frac{\Psi(p/p_0)}{(2\,\pi\,\hbar)^3} = \frac{p_0^3}{2\,\pi^2\,\hbar^3}\ \int_0^\infty x^2\ dx\ \Psi(x)$$

We can thus write the phase space distribution function as

$$f(\vec{r},\vec{p}) = n(\vec{r})\ \frac{2\,\pi^2\,\hbar^3}{p_0^3}\ \psi\left(\frac{p}{p_0}\right)\ , \tag{A.1}$$

where the function

$$\psi(x) \equiv \Psi(x)\ \frac{p_0^3}{2\,\pi^2\,\hbar^3}\quad ,\quad x = \frac{p}{p_0}\ ,$$

is normalized by

$$\int_0^\infty x^2\, dx\, \psi(x) = 1\ .$$

The Pauli principle imposes the bound eq.(9) which combined with eq.((A.1) yields,

$$n(\vec{r}) \leq \frac{p_0^3}{\hbar^3\, \pi^2\, \psi(p/p_0)}\ .$$

Since the momentum distribution $\psi(p/p_0)$ is normally a monotonically decreasing function of p, the most stringent bound is obtained setting $p = 0$:

$$n(\vec{r}) \leq \frac{p_0^3}{\hbar^3\, \pi^2\, \psi(0)} = \frac{\sqrt{27}\, m^3\, \sigma^3}{\hbar^3\, \pi^2\, \psi(0)}\ . \tag{A.2}$$

Therefore, the phase space density eq.(13) is bounded by

$$Q(\vec{r}) \leq K\, \frac{m^4}{\hbar^3}\ , \tag{A.3}$$

where the dimensionless quantity K is given by

$$K \equiv \frac{\sqrt{27}}{\pi^2\, \psi(0)} \tag{A.4}$$

The value of K depends on the nature of the momentum distribution.

For DM particles in thermal equilibrium p_0 is equal to the temperature T and

$$\Psi(x) = \frac{1}{e^x + 1}\ . \tag{A.5}$$

For sterile neutrinos in the ν-MSSM model [52] which decouple out of equilibrium. Their freezed-out distribution function $\Psi(x)$ is given by [8]

$$\Psi(x) = 2\, \tau\, \sqrt{\frac{\pi}{x}} \sum_{n=1}^{\infty} \frac{e^{-n\, x}}{n^{\frac{5}{2}}}\ . \tag{A.6}$$

where $\tau \simeq 0.03$ is a coupling constant. This formula is valid for all $\sqrt{x} > \tau$ and we take $\Psi(x) = 1$ for $\sqrt{x} < \tau$.

For sterile neutrinos in the Dodelson-Widrow model [21] we have (approximately) the freezed-out distribution function

$$\Psi(x) = \frac{f_0}{m}\, \frac{1}{e^x + 1} \quad \text{where} \quad f_0 \simeq 0.043\ \text{keV}\ . \tag{A.7}$$

We display K in Table 1 for thermal fermions, out of thermal equilibrium fermions in the DW and ν-MSM models and for the Maxwell-Boltzmann distribution.

Notice that the quantum bound is more restrictive (K turns to be smaller) in the out of thermal equilibrium ν-MSM model than in the other cases. This is due to the fact that generically, out of equilibrium distributions as the ν-MSM have more particles with low momentum [6, 16]. $\psi(0)$ is therefore larger than at thermal equilibrium and from eq.(A.4) K is smaller.

The equilibrium Fermi-Dirac distribution produces the less restrictive bound in Table 1 because, somehow, it already knows about the exclusion principle.

References

[1] Y Ascasibar and S. Gottlöber, MNRAS, 386, 2022 (2008).
[2] V. Avila-Reese et al., Ap J, 559, 516 (2001).
[3] N. Bilic, R. D. Viollier, Phys. Lett. B408, 75 (1997) and Eur. Phys. J. C11:173 (1999).
[4] A. Bonasera et al. Phys. Rev. Lett. 71, 505 (1993).
[5] A. Bonasera, Phys. Rep. 243, 1 (1994).
[6] D. Boyanovsky, C. Destri, H. J. de Vega, Phys. Rev. **D 69**, 045003 (2004).
[7] D. Boyanovsky, H. J. de Vega, N. G. Sanchez, arXiv:0710.5180, Phys. Rev. **D 77**, 043518 (2008).
[8] D. Boyanovsky, Phys. Rev. D78:103505, (2008).
[9] J. P. Brodie et al., The Astronomical Journal 142, 199 (2011).
[10] P. H. Chavanis, Phys. Rev. **E65**, 056123 (2002),
[11] P. H. Chavanis, Int. J. Mod. Phys. B20, 3113 (2006).
[12] P. Colín, O. Valenzuela, V. Avila-Reese, Ap J, 542, 622 (2000).
[13] P. Colín, O. Valenzuela, V. Avila-Reese, Ap J, 673, 203 (2008).
[14] J. J. Dalcanton, C. J. Hogan, Astrophys. J.**561**, 35 (2001).
[15] W. J. G. de Blok, Advances in Astronomy, vol. 2010, pp. 1-15, arXiv:0910.3538.
[16] C. Destri, H. J. de Vega, Phys. Rev. **D 73**, 025014 (2006).
[17] C. Destri, H. J. de Vega, M. Lattanzi, N. G. Sanchez, in preparation.
[18] H. J. de Vega, N. G. Sánchez, arXiv:0901.0922, Mon. Not. R. Astron. Soc. **404**, 885 (2010).
[19] H. J. de Vega, P. Salucci, N. G. Sanchez, arXiv:1004.1908, New Astronomy **17**, 653 (2012), and references therein.
[20] H. J. de Vega, N. G. Sánchez, Phys. Rev. D85, 043516 (2012) and D85, 043517 (2012).
[21] S. Dodelson, L. M. Widrow, Phys. Rev. Lett. **72**, 17 (1994).
[22] F. Donato et al., MNRAS **397**, 1169 (2009).
[23] L. Gao and T. Theuns, Science, 317, 1527 (2007).
[24] G. Gilmore et al., Ap J, 663, 948 (2007).
[25] D. Gorbunov, A. Khmelnitsky, V. Rubakov, JCAP 0810:041 (2008).
[26] D S Gorbunov, V A Rubakov, *Introduction to the theory of the early universe*, World Scientific, 2011, Singapore.
[27] Y. Hoffman et al. Ap J, 671:1108 (2007).
[28] C. J. Hogan, J. J. Dalcanton, Phys. Rev. **D62**, 063511 (2000),
[29] H. S. Köhler, Nucl. Phys. A400, 233c (1983).
[30] J Kormendy, K C Freeman, IAU Symposium, Sydney, 220, 377 (2004), arXiv:astro-ph/0407321.
[31] L D Landau and E M Lifshits, Statistical Mechanics, Elsevier, Oxford, 1980.
[32] L D Landau and E M Lifshits, Quantum Mechanics, Elsevier, Oxford, 1977.
[33] A. Lapi, A. Cavaliere, Ap J, 743, 127 (2011).
[34] R. B. Larson, MNRAS, 145, 405 (1969) and 147, 323 (1970).
[35] H. W. Lee, Phys. Rept. 259, 147 (1995).
[36] M. R. Lovell et al., MNRAS, 420, 2318 (2012).
[37] A. Ludlow et al. MNRAS, 415, 3895 (2011).
[38] A. V. Macciò, S. Paduroiu, D. Anderhalden, A. Schneider, B. Moore, MNRAS, 424, 1105 (2012).
[39] J. Madsen, Phys. Rev. Lett. **64**, 2744 (1990).
[40] J. Madsen, Phys. Rev. **D64**, 027301 (2001).
[41] N. F. Martin et al. ApJ 684, 1075 (2008).
[42] G. D. Martinez et al., Ap J, 738, 55 (2011).
[43] E. Memola et al., A & A, Volume 534, A50 (2011).
[44] F. Munyaneza, P. L. Biermann, A & A, 458, L9 (2006).
[45] J. F. Navarro et al. MNRAS, 402, 21 (2010).
[46] S. H. Oh et al., Astronomical Journal, 136, 2761 (2008).
[47] E. Papastergis et al., Ap J, 739, 38 (2011).
[48] M. Persic et al., MNRAS, 281, 27 (1996).
[49] P. Salucci et al., MNRAS, 378, 41 (2007).
[50] P. Salucci, Ch. Frigerio Martins, arXiv:0902.1703, EAS Publications Series, 36, 2009, 133-140.
[51] S. Shao, L. Gao, T. Theuns, C. S. Frenk, arXiv:1209.5563.
[52] M. Shaposhnikov, I. Tkachev, Phys. Lett. B639, 414 (2006).
[53] J. D. Simon, M. Geha, Ap J, 670, 313 (2007) and references therein.
[54] J. D. Simon et al., Ap. J. 733, 46 (2011) and references therein.
[55] Z. Slepian, J. Goodman, arXiv:1109.3844, to appear in MNRAS.
[56] J. Sommer-Larsen, A. Dolgov, Ap J, 551, 608 (2001).
[57] M. Spano et al., MNRAS, 383, 297 (2008).

[58] A. V. Tikhonov et al., MNRAS, 399, 1611 (2009).
[59] S. Tremaine, J. E. Gunn, Phys. Rev. Lett. 42, 407 (1979).
[60] S. Tremaine, M. Henon, D. Lynden-Bell, Mon. Not. Roy. Astron. Soc. **219**, 285 (1986).
[61] J. van Eymeren et al. A & A 505, 1-20 (2009).
[62] I. M. Vass et al., Mon. Not. R. Astron. Soc. **395**, 1225 (2009).
[63] F. Villaescusa-Navarro and N. Dalal, JCAP 03, 024 (2011).
[64] J. Viñas, E. Salvador-Solé, A. Manrique, MNRAS 424, L6 (2012).
[65] M. Walker, J. Peñarrubia, Ap. J. 742, 20 (2011).
[66] Matthew Walker, private communication.
[67] B. Willman and J. Strader, The Astronomical Journal, 144, 76 (2012).
[68] J. Wolf et al., MNRAS, 406, 1220 (2010) and references therein.
[69] C-Y Wong, Phys. Rev. C25, 1460(1982).
[70] J. Woo et al. MNRAS, 390, 1453 (2008).
[71] R. F. G. Wyse, G. Gilmore, IAU Symposium, Vol. 244, p. 44-52 (2007), arXiv:0708.1492.
[72] J. Zavala et al., Ap J, 700, 1779 (2009).